Volume 1 | Number 1 | Jan 2013 | Pages 1–100

ChemComm

Chemical Communications
www.rsc.org/chemcomm

ROYAL SOCIETY OF CHEMISTRY

ROYAL SOCIETY OF CHEMISTRY

www.rsc.org/chemcomm

Chemical Communications

COMMUNICATION

Plasmonic biocompatible silver-gold alloyed nanoparticles

Georgios A. Sotiriou[a,b], Gion Diego Etterlin[a], Anastasia Spyrogianni[a], Frank Krumeich[a], Jean-Christophe Leroux[c], Sotiris E. Pratsinis[a*]

The addition of Au during scalable synthesis of nanosilver drastically minimizes its surface oxidation and leaching of toxic Ag$^+$ ions. These biocompatible and inexpensive silver-gold nanoalloyed particles exhibit superior plasmonic performance over that of commonly–used pure Au nanoparticles and as such these nanoalloys have great potential in theranostic applications.

The plasmon resonance of metallic nanoparticles makes them attractive for biomolecule sensing in disease diagnosis[1] and/or therapeutic interventions due to their efficient light-into-heat photothermal conversion.[2] Among plasmonic nanoparticles, most research has been focused on gold and silver.[3] Both have their plasmon resonance frequency in the visible spectrum. Silver, however, exhibits intrinsically stronger plasmonic performance than gold because of its lower losses in the UV and visible spectrum.[4]

On the other hand, the silver surface easily oxidizes at ambient conditions[5] reducing its plasmonic performance.[6] Alloyed silver-gold nanoparticles, however, resist surface oxidation and may be employed in plasmonic applications such as surface-enhanced Raman scattering (SERS).[7] Furthermore, silver nanoparticles (nanosilver) can be toxic[8] due to the rapid dissolution of their surface oxide layer and release of Ag$^+$ ions.[9] This prohibits the use of nanosilver in biomedical applications where inert materials are sought.[10] As a result, research in biomedical applications focuses mostly on the plasmonically inferior and rather expensive gold. Therefore, there is a need for inexpensive and non-toxic plasmonic nanoparticles.

One way to minimize the toxicity of silver nanoparticles is to hermetically encapsulate them with non-toxic amorphous silica.[11] That way both Ag$^+$ ion release, as well as direct nanosilver contact with biological systems are reduced. However, often the bare metallic surface is needed for the specific attachment of biomolecules.[1] An alternative approach is surface sulfidation of nanosilver that also minimizes the release of Ag$^+$ ions[12] and reduces its toxicity and environmental impact. Sulfidation, however, destroys silver's plasmonic performance.[13] Therefore, the challenge still remains to fabricate silver-based plasmonic nanoparticles with minimal toxic Ag$^+$ ion release but without any coating.

Here, we rationally design and form plasmonic silver-gold nanoalloys (0-100 at% Au content) and systematically measure their plasmonic resonance, release of Ag$^+$ ions and cytotoxicity *in vitro*.

We specifically investigate the effect of Au alloying in rather small (<10 nm) Ag nanoparticles since in these sizes the *in vitro* toxicity is dominated by the released Ag$^+$ ions.[14-15] It has been observed that the antibacterial activity and toxicity of Ag-Au alloyed nanoparticles decreases nonlinearly with increasing Au content.[16-18] To better understand this, such nanoalloys with closely controlled composition are made here by flame aerosol technology.[14] This is a scalable process (up to kg/h) for manufacturing of nanomaterials with several advantages including no liquid by-product generation and facile collection of particles with unique morphology and high purity (e.g. optical fibres).[19] This last property is especially useful for studying biological interactions as it minimizes undesired nanoparticle surface contamination.[20] So, a liquid precursor solution is atomized and *in situ* pyrolyzed resulting in Ag-Au nanoparticles immobilized on nanosilica (schematic in Figure 1, upper left corner).[21] The presence of SiO$_2$ prevents metallic particle agglomeration and flocculation in both aqueous[14] and high salt-content solution,[22] as no nanoparticle surface functionalization is used that could compromise or interfere with the metal ion release kinetics. Here, all Ag, Au and Si precursors are present in the initial flammable precursor solution. Nanostructured SiO$_2$ particles are formed first in the flame followed by the metallic nanoparticles due to the higher SiO$_2$ boiling point than that of both gold and silver.[23] That way, metallic nanoparticles are attached onto the nanostructured SiO$_2$ support with high exposed surface area,[9] similarly to noble metal clusters on ceramics in heterogeneous catalysis.[24] The metallic particle size and the Ag-Au composition can be tuned by the flame aerosol process conditions and precursor solution composition.[14,21,25] The metallic content (Ag and Au) is set here at 50 wt%.

Figure 1 shows high resolution high-angle annular dark field scanning transmission electron microscopy (HAADF-STEM or Z contrast STEM) images (a,b) of Au-Ag (50 at% Au content) nanoparticles that appear as bright spots because of their high proton (Z) number. The diffuse gray areas correspond to the amorphous SiO$_2$ support.[26] Figure 1c shows an image using a small bright field detector for phase-contrast[27] of the same nanoparticles where Ag and Au appear darker showing their crystal lattices and verifying the presence of nanocrystals. The focused electron beam can be set on the center of a single nanoparticle (red spot in Figure 1a). The
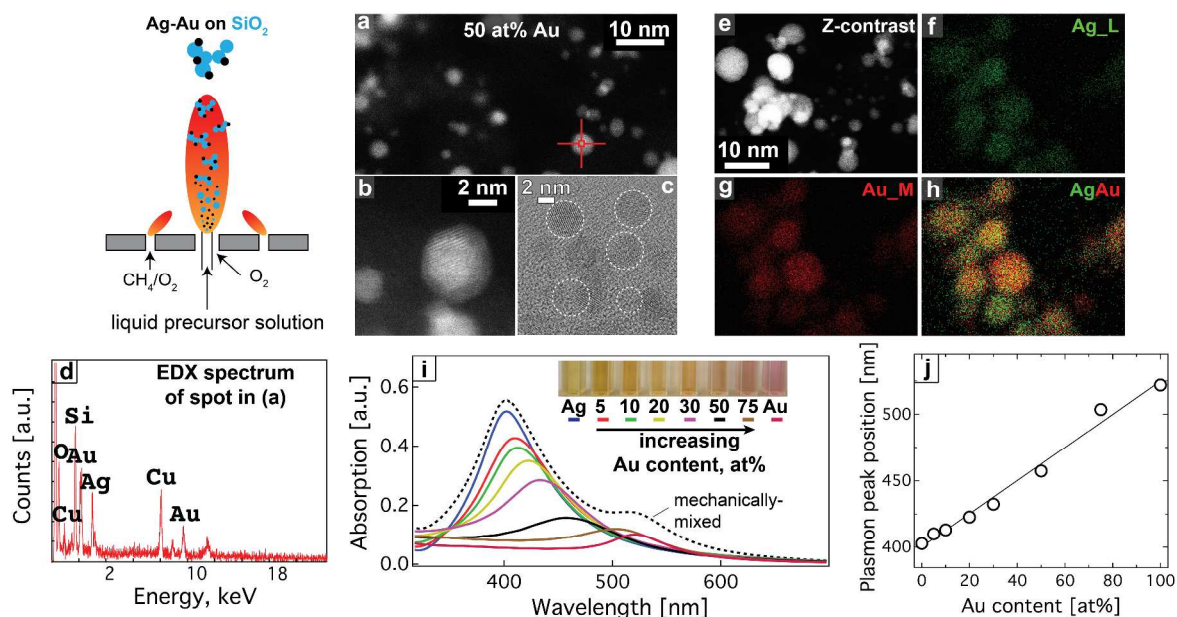
Fig. 1 Schematic diagram of the flame spray pyrolysis process (upper left corner). High resolution high-angle annular dark field scanning transmission electron microscopy (HAADF-STEM) images (a,b) and an image using a small bright field phase-contrast detector (c) of Au-Ag (50 at% Au content) nanoparticles. (d) Energy dispersive X-ray (EDX) spectrum of spot in (a). (e) HAADF-STEM image of the same sample, and its elemental mapping for Ag (f), Au (g) and both elements merged (h). (i) The optical absorption of aqueous suspensions containing the Ag-Au nanoalloy particles (10 mg/L of metal) for increasing Au content (solid lines) as well as one mechanically-mixed sample (broken line, equivalent to 50 at% Au). (j) The peak position of each spectrum from (i) is plotted as a function of Au at%.

energy dispersive X-ray (EDX) spectrum of that spot reveals the local elemental composition (Figure 1d) that consists of Ag, Au and Si. The simultaneous presence of Ag and Au in a single nanoparticle indicates nanoalloy formation.[26] The Cu and C peaks (Figure 1d) originate from the carbon-coated copper grid. Figure 1 further shows a HAADF-STEM image (e) of the same sample, and its elemental mapping for Ag (f), Au (g) and both elements merged (h). Both Ag and Au are interspaced within each particle indicating their co-existence and alloyed form there and there is some fluctuation in the Ag-Au ratio in each nanoparticle.

To further verify Ag-Au nanoalloy formation, the optical absorption of aqueous suspensions containing these nanoparticles (10 mg/L of metal) is shown in Figure 1i for increasing Au content (solid lines) along with a mechanically-mixed sample (broken line, equivalent to 50 at% Au). All flame-made samples exhibit a single band with their peak position ranging from 400 nm (for pure Ag) to 525 nm (for pure Au)[28-29] and the color of the aqueous suspensions shifts respectively from bright yellow to red (inset), while their absorbance width corresponds well to their narrow particle size distributions (SI, Figure S1).[28-30] The intensity decreases for increasing Au content because of the different extinction coefficients of each metal.[28] In contrast, the absorption spectrum of the mechanically-mixed sample exhibits two distinct peaks at the corresponding positions for each metal. This proves the nanoalloy formation at all Au contents.[3,28-29] In fact, if the peak position of each spectrum is plotted as a function of Au at% (Figure 1j), the data follow a linear dependency consistent with literature,[3,28-29] indicating the formation of overall homogeneous Ag-Au nanoparticles at all compositions.[28-29]

The average size as determined by electron microscopy for pure Ag and Au nanoparticles is 8 and 14 nm, respectively (Supporting Information-SI, Figure S1). Such metallic nanoparticle sizes can be made by various wet- or gas-phase techniques.[18,26,28-29,31] Interestingly, increasing the Au content during particle synthesis slightly decreases the average metallic size to 4-6 nm up to 50 at% of Au. This indicates that the presence of Au during Ag nanoparticle

synthesis inhibits the resulting alloy nanoparticle growth similar to the formation of solid solutions in ceramics.[32] This is also shown by the X-ray diffraction patterns of those nanoparticles (SI, Figure S2a) in which the XRD peaks of nanoalloys broaden upon Au addition indicating a smaller crystal size.

The release of Ag^+ ions from nanoalloys (0-100 at% Au content) in air-saturated water after equilibrium[9] is shown in Figure 2a (open circles) as a function of the Au content (at%) for a total metal (Ag & Au) concentration of 100 mg/L. Pure nanosilver releases 18 mg/L Ag^+ ions which is equal to 18% of its total mass, in agreement with literature for flame-made nanosilver of 8 nm crystal size.[14] For increasing Au content, however, the Ag^+ ion release becomes minimal and above 30 at% Au, the release of Ag^+ ions becomes identical to that from the control sample (100 at% Au content).

The mechanically-mixed Ag-Au samples (filled circles) exhibit much higher Ag^+ ion release than that of the nanoalloys (open circles) for equivalent Au content and similar to that of pure nanosilver for that size.[14] Therefore, the reduced Ag^+ ion release from nanoalloys is attributed to the presence of Au that minimizes Ag oxidation. In fact, the metallic particle size in the nanoalloys is smaller than that of pure Ag (SI, Figure S2b), therefore, the Ag^+ ion release should have been even higher (e.g. ~70 wt% for 4 nm flame-mage Ag crystals on SiO_2).[14] It should be emphasized that the minimal Ag^+ ion release from the Ag-Au nanoparticles is not attributed to the progressively lower amount of Ag that is present in the nanoalloys. The Ag^+ ion release % (Ag as Ag^+ ions, normalized to the total Ag content) for all Ag-Au nanoalloys (0-75 at% Au) also decreases for increasing Au content (SI, Figure S3). If the alloying with Au would have no effect on the Ag^+ ion release, all nanoalloys should exhibit similar values. In contrast, the mechanically-mixed Ag-Au samples retain their high Ag^+ ion release % that corresponds to pure nanosilver particles as stated just above.

Figure 2b shows the plasmon peak position difference $\Delta\lambda$ of all nanoalloys in ethanol and water as a function of Au content. The $\Delta\lambda$ drastically decreases for increasing Au content. In the insets, the
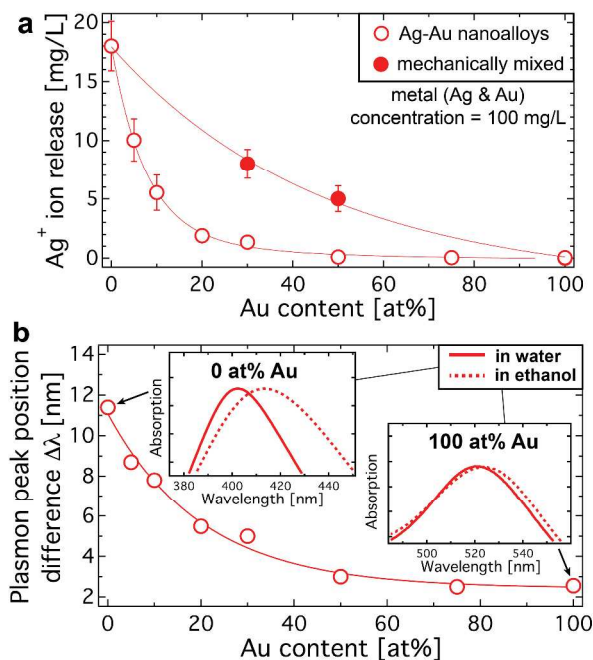
Fig. 2 (a) The Ag$^+$ ion release of nanoalloys (0-100 at% Au content) in water (open circles) as a function of the Au content (at%) (total noble metal concentration of 100 mg/L). (b) The plasmon peak position difference Δλ of all nanoalloys in ethanol and water as a function of Au content. In insets, the absorption spectra of pure Ag and Au in water (solid lines) and ethanol (broken lines) are shown.

absorption spectra of pure Ag and Au in water (solid lines) and ethanol (broken lines) are shown. The nanosilver metallic surface is in direct contact with water in aqueous solutions because any silver oxide surface layer present during flame synthesis of Ag-Au nanoparticles on SiO$_2$ has been dissolved rapidly.[9] However, in alcoholic solutions such silver oxide layers do not dissolve[33] and thus the Ag metallic surface is still covered by an oxide layer. The plasmon absorption band of metallic nanosilver is sensitive to its environment exhibiting a red-shift for a surrounding material with an increased refractive index.[34] Silver oxide has a higher refractive index than water and thus, this silver oxide surface layer can be detected by monitoring the shift of the optical absorption spectra in alcohol and in water (with and without the oxide surface layer, respectively): for increased silver oxide fraction the shift Δλ increases.[35] Therefore, the Au nanoalloying in nanosilver reduces the surface Ag$_2$O layer formation, as has been seen also for other Ag-Au nanoalloys.[7,36] Extended X-ray absorption fine structure (EXAFS) analysis of identical flame-made Ag-Au nanoalloys (50 at% Au) has further highlighted that Ag is less oxidized in this bimetallic rather than its monometallic form.[26] The charge transfer between Au and Ag in the nanoalloys is also investigated here by X-ray photoelectron spectroscopy (SI, Figure S4), further verifying the nanoalloy formation.

The cytotoxicity of nanosilver at these sizes (~10 nm) originates mostly from the released Ag$^+$ ions from its oxidized surface.[21] Therefore, it is anticipated that the cytotoxicity of the nanoalloys should progressively decrease for an increasing Au content. This is examined here against murine macrophages that serve as a model cell line since these cells will be likely the most exposed to nanoparticles following systemic exposure in mammals. Nanoparticles are generally cleared from the systemic circulation by the mononuclear phagocyte system.[37]

The nanoparticle *in vitro* cytotoxicity is determined by monitoring the mitochondrial activity of these cells (SI, Materials

and Methods). We deliberately chose serum-free cell medium here to avoid any interference on the cytotoxicity mechanism by the presence of proteins.[21] Figure 3a shows the cell viability as a function of Au content in the presence of different nanoalloy concentrations (3.1-25 mg/L of metal). The control range (dotted lines) corresponds to the negative control experiment and its error bar. The nanoparticle cytotoxicity decreases with increasing Au content for all employed nanoparticle concentrations reaching values within the negative control range (dotted lines) for Au content >50 at%. In fact, for the highest nanoparticle concentration (25 mg/L of metal, black squares), the cell viability shifts from 10% (very toxic) for pure Ag (0 at% Au content) to >95% (benign) for 50 at% Au content. The cytotoxicity of pure Ag nanoparticles and their released Ag$^+$ ions are in agreement with the literature.[21] At higher concentrations all nanoparticle components induce cytotoxicity including pure SiO$_2$ (e.g. 40% cell viability at 100 mg/L and 100% cell viability at the 3-25 mg/L of Figure 3a).[21] Furthermore, when the same cell viability data are plotted as a function of Ag mass concentration for all Ag-Au nanoalloys (SI, Figure S5), the same effect is observed. At similar Ag mass concentrations, the nanoalloys exhibit higher cell viability than that of pure Ag. This highlights that nanosilver cytotoxicity can be drastically tuned by Au alloying that minimizes Ag surface oxide formation and subsequent Ag$^+$ ion release. This result essentially clarifies the non-linear dependency between Ag$^+$ ion release and cytotoxicity from Ag-Au alloys.[16-17,38]

The biomedical potential of such nanoalloys is demonstrated with their photothermal performance. Nanocomposite pellets containing 2.5 wt% of each nanoalloy are irradiated with a near-IR laser (λ = 785 nm, 15 W/cm^2 flux, spot size 5 mm) and their temperature is monitored over time. The metallic particles are brought in close proximity inside the pressed pellet simulating the controlled plasmonic coupling in nanoaggregates[39] that broadens their optical absorption to the near-IR range converting that irradiation to heat. Figure 3b shows the ΔT$_{max}$ achieved after 3 min
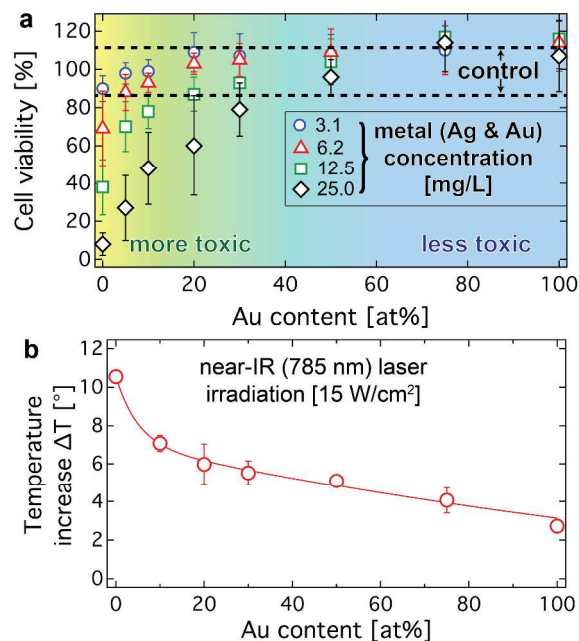

Fig. 3 (a) The cell viability of murine macrophages as a function of Au content in the presence of different nanoalloy concentrations (3.1-25 mg/L of metal). (b) The ΔT$_{max}$ achieved after 3 min of continuous laser irradiation (λ =785 nm, 15 W/cm^2 flux, spot size 5 mm) of nanocomposite pellets containing the nanoalloy particles.

of laser irradiation as a function of Au content in the nanoalloy particles. The absorption cross-section of pure Ag is higher than that of pure Au and their alloys,[28] therefore, it is expected to outperform all of them here. However, the ΔT_{max} of nanoalloys with Au content 30-50% that exhibit minimal cytotoxicity (Figure 3a) achieve 2-3 times higher performance than pure Au nanoparticles. This indicates that Ag-Au nanoalloys are advantageous over commonly used Au particles at similar architectures or morphologies in such biomedical applications.

In summary, we demonstrate how the fundamental understanding of the Ag^+ ion release mechanism can be exploited to engineer safer and inexpensive, nanosilver-based, plasmonic nanoparticles. By adding Au during nanoparticle synthesis, homogeneous Ag-Au nanoalloys are formed that finely control the metal surface oxidation and any Ag^+ ion release in aqueous solutions. This alloying renders such nanoparticles less cytotoxic so their superior plasmonic properties could be investigated when arranged in suitable architectures (e.g. nanoaggregates, nanoshells, nanocubes) for biomedical applications prompting for further investigations regarding their *in vivo* stability at various pH.[40]

Notes and references

[a] Particle Technology Laboratory, Institute of Process Engineering, Department of Mechanical and Process Engineering, ETH Zurich, Sonneggstrasse 3, Zurich 8092, Switzerland.
[b] Molecular and Integrative Physiological Sciences, Department of Environmental Health, School of Public Health, Harvard University, 665 Huntington Ave., Boston, MA 02115, USA.
[c] Drug Formulation & Delivery, Institute of Pharmaceutical Sciences, Department of Chemistry and Applied Biosciences, ETH Zurich, Wolfgang-Pauli-Strasse 10, Zurich 8093, Switzerland.
*Corresponding author: sotiris.pratsinis@ptl.mavt.ethz.ch

1. J. N. Anker, W. P. Hall, O. Lyandres, N. C. Shah, J. Zhao, R. P. Van Duyne, *Nat. Mater.*, 2008, **7**, 442-453.
2. E. C. Dreaden, A. M. Alkilany, X. Huang, C. J. Murphy, M. A. El-Sayed, *Chem. Soc. Rev.*, 2012, **41**, 2740-2779.
3. M. B. Cortie, A. M. McDonagh, *Chem. Rev.*, 2011, **111**, 3713-3735.
4. W. L. Barnes, A. Dereux, T. W. Ebbesen, *Nature*, 2003, **424**, 824-830.
5. O. S. Ivanova, F. P. Zamborini, *J. Am. Chem. Soc.*, 2010, **132**, 70-72.
6. Y. Han, R. Lupitskyy, T.-M. Chou, C. M. Stafford, H. Du, S. Sukhishvili, *Anal. Chem.*, 2011, **83**, 5873-5880.
7. H. Lee, Y. Yoo, T. Kang, J. In, M.-K. Seo, B. Kim, *Small*, 2012, **8**, 1527-1533.
8. S. M. Hussain, K. L. Hess, J. M. Gearhart, K. T. Geiss, J. J. Schlager, *Toxicol. Vitro*, 2005, **19**, 975-983.
9. G. A. Sotiriou, A. Meyer, J. T. N. Knijnenburg, S. Panke, S. E. Pratsinis, *Langmuir*, 2012, **28**, 15929-15936.
10. G. A. Sotiriou, S. E. Pratsinis, *Curr. Opin. Chem. Eng.*, 2011, **1**, 3-10.
11. G. A. Sotiriou, T. Sannomiya, A. Teleki, F. Krumeich, J. Vörös, S. E. Pratsinis, *Adv. Funct. Mater.*, 2010, **20**, 4250-4257.
12. C. Levard, E. M. Hotze, B. P. Colman, A. L. Dale, L. Truong, X. Y. Yang, A. J. Bone, G. E. Brown, Jr., R. L. Tanguay, R. T. Di Giulio, E. S. Bernhardt, J. N. Meyer, M. R. Wiesner, G. V. Lowry, *Environ. Sci. Technol.*, 2013, **47**, 13440-13448.
13. L. Wang, W. Xiong, Y. Nishijima, Y. Yokota, K. Ueno, H. Misawa, G. Bi, J.-r. Qiu, *Opt. Express*, 2011, **19**, 10640-10646.
14. G. A. Sotiriou, S. E. Pratsinis, *Environ. Sci. Technol.*, 2010, **44**, 5649-5654.
15. Z.-m. Xiu, Q.-b. Zhang, H. L. Puppala, V. L. Colvin, P. J. J. Alvarez, *Nano Lett.*, 2012, **12**, 4271-4275.
16. D. Mahl, J. Diendorf, S. Ristig, C. Greulich, Z.-A. Li, M. Farle, M. Koeller, M. Epple, *J. Nanopart. Res.*, 2012, **14**.
17. D. Tiedemann, U. Taylor, C. Rehbock, J. Jakobi, S. Klein, W. A. Kues, S. Barcikowski, D. Rath, *Analyst*, 2014, **139**, 931-942.
18. S. Grade, J. Eberhard, J. Jakobi, A. Winkel, M. Stiesch, S. Barcikowski, *Gold Bull.*, 2014, **47**, 83-93.
19. S. E. Pratsinis, *AIChE J.*, 2010, **56**, 3028-3035.
20. S. Pokhrel, A. E. Nel, L. Madler, *Acc. Chem. Res.*, 2013, **46**, 632-641.
21. A. Pratsinis, P. Hervella, J.-C. Leroux, S. E. Pratsinis, G. A. Sotiriou, *Small*, 2013, **9**, 2576-2584.
22. G. A. Sotiriou, A. M. Hirt, P. Y. Lozach, A. Teleki, F. Krumeich, S. E. Pratsinis, *Chem. Mater.*, 2011, **23**, 1985-1992.
23. L. Madler, W. J. Stark, S. E. Pratsinis, *J. Mater. Res.*, 2003, **18**, 115-120.
24. R. Strobel, W. J. Stark, L. Madler, S. E. Pratsinis, A. Baiker, *J. Catal.*, 2003, **213**, 296-304.
25. L. Madler, S. E. Pratsinis, *J. Am. Ceram. Soc.*, 2002, **85**, 1713-1718.
26. S. Hannemann, J. D. Grunwaldt, F. Krumeich, P. Kappen, A. Baiker, *Appl. Surf. Sci.*, 2006, **252**, 7862-7873.
27. F. Krumeich, E. Mueller, R. A. Wepf, *Micron*, 2013, **49**, 1-14.
28. S. Link, Z. L. Wang, M. A. El-Sayed, *J. Phys. Chem. B*, 1999, **103**, 3529-3533.
29. M. P. Mallin, C. J. Murphy, *Nano Lett.*, 2002, **2**, 1235-1237.
30. X. Huang, X. Wang, X. Wang, X. Wang, M. Tan, W. Ding, X. Lu, *J. Catal.*, 2013, **301**, 217-226.
31. A. Q. Wang, J. H. Liu, S. D. Lin, T. S. Lin, C. Y. Mou, *J. Catal.*, 2005, **233**, 186-197.
32. S. Vemury, S. E. Pratsinis, *J. Am. Ceram. Soc.*, 1995, **78**, 2984-2992.
33. C. B. Wang, G. Deo, I. E. Wachs, *J. Phys. Chem. B*, 1999, **103**, 5645-5656.
34. K. A. Willets, R. P. Van Duyne, *Annu. Rev. Phys. Chem.*, 2007, **58**, 267-297.
35. A. Yanase, H. Komiyama, *Surf. Sci.*, 1992, **264**, 147-156.
36. S. Besner, M. Meunier, *J. Phys. Chem. C*, 2010, **114**, 10403-10409.
37. N. Bertrand, J.-C. Leroux, *J. Control. Release*, 2012, **161**, 152-163.
38. N. Alissawi, V. Zaporojtchenko, T. Strunskus, I. Kocabas, V. S. K. Chakravadhanula, L. Kienle, D. Garbe-Schoenberg, F. Faupel, *Gold Bull.*, 2013, **46**, 3-11.
39. G. A. Sotiriou, F. Starsich, A. Dasargyri, M. C. Wurnig, F. Krumeich, A. Boss, J.-C. Leroux, S. E. Pratsinis, *Adv. Funct. Mater.*, 2014, **24**, 2818-2827.
40. A. M. Goodman, Y. Cao, C. Urban, O. Neumann, C. Ayala-Orozco, M. W. Knight, A. Joshi, P. Nordlander, N. J. Halas, *ACS Nano*, 2014, **8**, 3222-3231.